www.czasopisma.pan.pl PAN POLSKA AKADEMIA NAUK www.journals.pan.pl

Arch. Min. Sci. **69** (2024), 1, 141-154

Electronic version (in color) of this paper is available: http://mining.archives.pl

DOI: https://doi.org/10.24425/ams.2024.149833

ZHIQIANG YIN[1*], CHAO WANG[1], ZHIYU CHEN[2], YOUXUN CAO[3], TAO YANG[3], DEREN CHEN[4], DENGKE WANG[4]

STUDY ON MECHANICAL RESPONSE CHARACTERISTICS OF ANCHOR UNDER DYNAMIC DISTURBANCE

The roadway surrounding rock is often subjected to severe damage under dynamic loading at greater mining depths. To study the dynamic response of prestressed anchors, the damage characteristics of anchor solids with different prestresses and number of impacts under dynamic and static loads were investigated by improving the Hopkinson bar equipment. The effect of prestress on stress wave transmission was obtained, and the laws and reasons for axial force loss under static and dynamic loads were analyzed. The damage characteristics of anchor solids were determined experimentally. The results show that with an increase in prestress from 15 to 30 MPa, the peak value of the stress wave gradually increases and the decay rate gradually decreases. Shear damage occurred at the impact end of the specimen, combined tension and shear damage occurred at the free end, and fracture occurred in the middle. With an increase in the number of impacts, the damage to the anchor solid specimens gradually increased, and the prestressing force gradually decreased. After impact, the axial force of the various prestressed anchor solid specimens gradually increased; however, the anchor bar with a 17 MPa prestressing force had the slowest rate of axial force loss during impact, withstanding a greater number of impacts. In on-site applications, after three explosions, the displacement on both sides of the tunnel supported by 17 MPa prestressed anchor rods could be controlled within 0.3 m, with an average displacement of 206, 240, and 283 mm, respectively, increasing by 16.5% and 17.9%. This study, based on theoretical analysis and laboratory research combined with field application provides guidance for the anchor support of a dynamic loading tunnel.

Keywords: anchor solid; prestressed; impact times; stress wave; damage of surrounding rock

[1] ANHUI UNIVERSITY OF SCIENCE AND TECHNOLOGY, SCHOOL OF MINING ENGINEERING, ANHUI PROVINCE COAL MINE SAFETY MINING EQUIPMENT MANUFACTURING INNOVATION CENTER, HUAINAN 232001, CHINA
[2] INDUSTRIAL AND ENERGY ADMINISTRATION OF XISHUI COUNTY, ZUNYI 564699, CHINA
[3] GREAT WALL NO.6 MINING CO. LTD, ETUOKEQIANQI 016200, CHINA
[4] SHANDONG HUAKUN GEOLOGICAL ENGINEERING CO. LTD, TAIAN 271413, CHINA

* Corresponding author: zhqyin@aust.edu.cn

1. Introduction

Anchor rods are an efficient and economical rock support technology that have been widely used in mines, tunnels, and various rock projects. With increasing mine depth, there are increasing complications in the ground stress of the rock surrounding the roadway. In deep mines, the loss of prestress and pretension of anchor rods is a prominent problem, and numerous field and laboratory tests, numerical simulations, and theoretical analyses have been conducted by researchers worldwide [1-4]. These research results are of great significance for gaining a deeper understanding of anchorage performance under static and quasi-static conditions; however, dynamic loading effects have not been sufficiently considered.

The stability of the anchor rod is restricted by the ground stress field of the mine and the deformation and failure characteristics of the surrounding rock as well as affected by the transient impact dynamic load on the anchor solid. With advancements in mining engineering and degree, the number and strength of roadway rockbursts caused by impact dynamic loads have increased, which considerably affects the support stability of deep roadways [5-7]. Kaiser [8] conducted a laboratory study to simulate the effect of an ejected rock mass on the dynamic mechanical characteristics of mechanical bolts during impact ground pressure; the friction anchors were found to be the ideal support method. Ansell [9] conducted free-fall tests on anchors in concrete cylinders to simulate environments such as rockbursts and detonating explosives and found that the distribution of plastic strain in grouted anchors along the length of the anchor was not constant. The portion allowed to yield plastically was not fully utilized in any case. Abdul-Hamid [10] conducted impact experiments on mechanical screw anchors using impulse-type loading and noted that the anchoring system had high load carrying capacity under high strain rate loading conditions with recommended values of 1.1 and 1.2 for anchor DIF. Drop tests on d-bolts were conducted by Charlie [11]; the energy absorption of the d-type anchor cross-section was observed to be directly proportional to the volume of the anchor cross-section, tensile strength of the anchor material, and ultimate strain. Solomos [12] conducted tensile tests on anchors in concrete with loading rates in the range of 75-225 MN/s using the Hopkinson rod technique and found that the force-displacement diagrams for dynamic loads were higher than those for the corresponding static loads. Wu [13] used SHPB to conduct impact tests on anchored parapet rock materials at a loading rate of 9 m/s to investigate the dynamic mechanical properties of rocks with different anchoring methods and anchor parapet angles. Some researchers have studied the influence of stress waves on the structural performance and mechanical response characteristics of anchor rods under dynamic loads using numerical simulations and theoretical analyses [14-16]. The above studies explored, to some extent, the influence of the force characteristics of anchor rods under dynamic loading; however, not enough consideration was given to prestressing. In engineering practice, the integrity and bearing capacity of the surrounding rock can be improved by prestressing anchor rods, which is beneficial for preventing anchor failure [17-20].

The aforementioned studies mainly analyzed the damage of anchors under dynamic loading, and less research on the mechanical response characteristics of anchor rods after impact under prestressing has been limited. In this study, an improved Hopkinson bar was adopted, different prestresses were applied to the anchor bar, and various impact tests with different numbers of impacts were conducted. The strain characteristics were monitored; fracture form, damage morphology, and dynamic response characteristics of the anchor bar along with the relationship

between the prestress and the number of impacts were studied. The application of these in the field is expected to provide a good solution for dynamic roadways.

2. Fabrication and test of test piece

2.1. Test piece production

In this experiment, dynamic strain gauges were used for strain monitoring; they were connected through the bridge box. Other components include data acquisition unit with LK2400N8 software, strain gauges (model BX120-1AA) pasted to the specimen using glue, with a resistance value of 120.6 ± 0.1 Ω, a sensitivity coefficient of 2.08 ± 1%, and a gate length × gate width of 1 mm × 0.5 mm, and the cement anchoring agent.

According to the basic theory of elastic waves, the design length of the test piece must be greater than the wavelength of the stress wave, which is approximately twice the length of a bullet (400 mm) in the SHPB test system. Therefore, the designed length of the test piece should not be less than 800 mm. The length of the rock surrounding the anchor solid used in the test was 1650 mm. The test piece used 42.5 cement, stones, and sand with particle sizes between 0.005-0.01 m as the production materials, with cement:sand:stone:water as 557:167:456:1270, and the outer diameter was 75 mm. A semi-through hole of 1500 mm length and 18 mm diameter was cut in it. The threaded steel bar of diameter 12 mm and length 1550 mm was selected for the anchor bolt. Strain gauges were used for strain monitoring. Strain gauges 1 and 2 were attached to the surrounding rock surfaces of the anchorage section, free section. Strain gauges 3 and 4 were attached and fixed to the anchor bolt. The test piece comprised an anchor bolt, anchor agent, rock surrounding the anchor solid, a sensor, an anchor plate, and a nut. The size and location of each component are shown in Fig. 1. A uniaxial mechanical test was conducted on an RMT-150C mechanical test bench. The mechanical parameters of the rock are listed in TABLE 1.

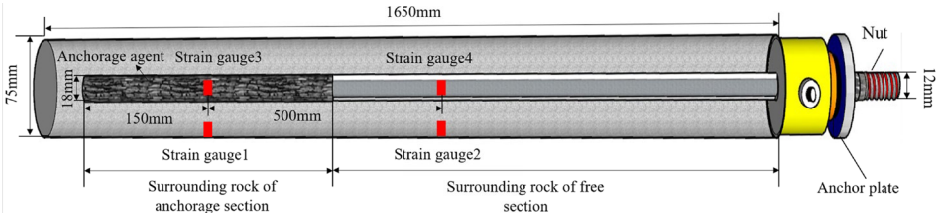

Fig. 1. Schematic diagram of anchor solid specimen

TABLE1

Concrete material parameters

Sample grade	Sample 1	Sample 2	Sample 3	Average
Compressive strength /MPa	33.62	30.08	29.89	31.53
Elastic modulus /GPa	27.8	25.8	28.4	27.3
Poisson's ratio	0.18	0.27	0.21	0.22

2.2. Test device

The test equipment used in this experiment consisted of an improved Hopkinson bar and a WAW-1000C testing machine. The improved Hopkinson pressure bar is shown in Fig. 2. The device primarily includes an incidence bar, transmission bar, bullet, and other components. In this experiment, the incident rod was 1500 mm long with a diameter of 75 mm. The sizes and materials of the transmission and incident rods were identical. Spindle-shaped bullets with a maximum diameter of 75 mm and length of 400 mm were used. They were made of the same material as the steel rod, to achieve half-sine wave loading and the waveform to achieve quantitative loading of the dynamic load. The strain input and maximum acquisition frequencies of the dynamic strain gauge were both 10 MHz.

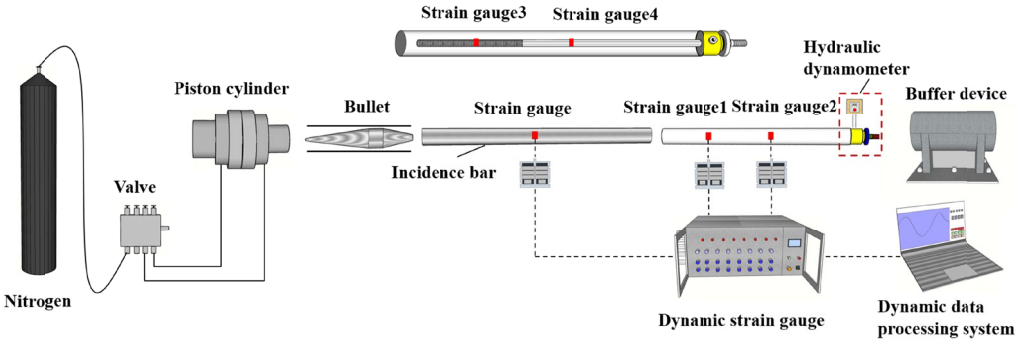

Fig. 2. Anchor solid dynamic load impact test system

2.3. Test conditions

Multiple impact tests were conducted on specimens prestressed with 15, 17, 25, and 30 MPa. During the test, the stress wave was monitored and the prestress of the bolt after each impact was recorded. The internal strain of the rock under a dynamic load can be calculated using the following equation [21]:

$$\varepsilon = \frac{v}{C_p} \tag{1}$$

Where: ε – is the strain value in the rock; v is the vibration velocity of rock particle, and the maximum value is 60 cm/s; C_p is the wave velocity of rock before blasting, taken as 1000 m/s. According to the test, when the pressure in the air gun was 0.2 MPa, the strain value in the incident rod was 314.5 με, and the strain value on the surrounding rock of anchor solid was 605.4 με; this aligned with the theoretical calculation results. Therefore, the use of 0.2 MPa air pressure can simulate the dynamic load action of the surrounding rock of the anchor solid well. Each test was completed when both ends of the test piece were damaged to the point where impact was not allowed or the axial force of the test piece was 0.

3. Test results and analysis

3.1. Analysis of influence of prestress on stress wave transmission

During the impact test, the prestressing force was applied using a torque wrench by adjusting the value of the main scale box differential scale to the required torque value. After adjustment, the locking ring was loosened, handle was locked automatically, prestressing force loading was completed, and impact was conducted using the same impact air pressure. The strain time course curves of the perimeter rock of the anchored section were obtained by monitoring strain gauge 1, as shown in Fig. 3. It can be observed that the first strain wave peak has a maximum value, and with an increase in time, the strain peak gradually decreases. With increasing prestress, the strain peak of the anchored section decreases gradually. Compared with the prestress conditions of 25 and 30 MPa, the stress wave decreases with time at 15 MPa, which indicates that the damage degree of the anchored solid is larger, and the stress wave decreases faster under low prestress conditions. With an increase in prestress, the peak strain of the surrounding rock in the anchored section decreases gradually.

The strain characteristic curves of the rock surrounding the free section under different prestresses were measured using strain gauge 2 installed on the rock surrounding the anchor solid. It can be seen from Fig. 4 that the first and second strain peaks are large under the 15 MPa prestress condition, and after the second strain peak, the strain values decrease significantly, indicating that the initial two large compression stress wave peaks cause certain damage to the surrounding rock of the free section, thus causing prestress loss. Under the prestress condition of 17 MPa, the strain in the surrounding rock in the free section gradually decreases, whereas in the attenuation stage, the peak value of the pressure strain is significantly higher than that of the tensile strain, indicating that the prestress is not completely eliminated under impact. Under the prestress condition of 25 MPa, the internal stress wave of the anchor body is superposed, rendering the second strain peak much larger than the first strain peak.

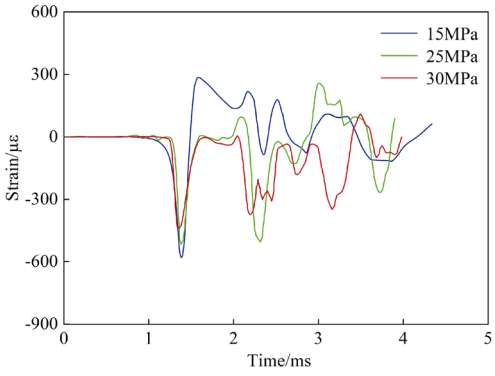

Fig. 3. Strain time history curve of surrounding rock in anchorage section

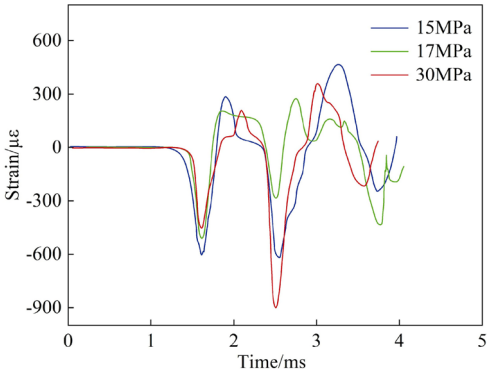

Fig. 4. Strain time history curve of surrounding rock in free section

3.2. Analysis of impact number on stress wave transmission

As shown in Fig. 5, a prestress of 15 MPa and an impact load of the same size were applied to the solid anchor specimen three times to obtain the strain characteristics of the rock surrounding the anchorage section. Under the prestress condition of 15 MPa, the peak stress increases with the increase in the number of impacts because the prestress in the anchor is lost with each impact. The action time of the first impact stress wave is longer than that of the next wave because the degree of damage in the anchor body is very low in the initial impact stage, whereas in the second impact stage, the damage accumulation of the anchor body accelerates the attenuation of the stress wave in the damaged area.

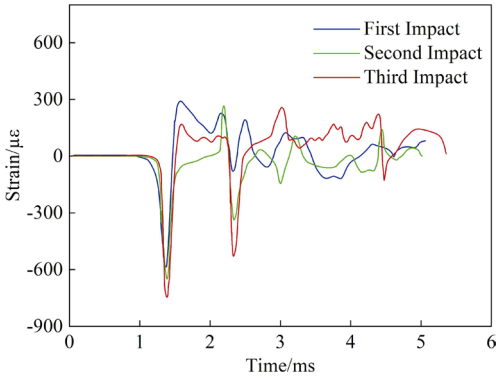

Fig. 5. Strain time history curves of anchorage section under multiple impacts

The surrounding rock of the free section was monitored under the action of 15 and 25 MPa prestresses and the strain characteristics of the surrounding rock of the free section under the action of the three impacts were obtained as shown in Fig. 6. Under a prestress condition of 15 MPa, the effect of the initial impact stress wave is evident and the surrounding rock in the free section exhibits a large tensile failure. With an increase in the number of impacts, the peak strain increases gradually. Under the condition of a 25 MPa prestress, the first peak strain of the surrounding rock in the free section gradually increases, which is the result of the joint action of the prestress loss and the failure of the surrounding rock of the anchor body. The rock surrounding the anchor body experiences a large compressive stress wave, whereas the tensile effect is small. In the rock surrounding the free section, increasing the prestress reduces the peak value of the stress wave under the initial impact. The size of the stress wave is related to the size of the prestress and to the degree of damage to the surrounding rock of the anchor. Furthermore, increasing the prestress in the anchor helps reduce the tensile stress wave effect in the anchor. The strain during the first impact of 15 MPa prestress was 606.9 με. Under the action of 25 MPa prestress, the strain during the first impact was relatively small at 441.4 με. The strain during the third impact under the action of 15 MPa prestress was 827.3 με which is an increase of 36.3% compared to that in the first impact. The strain value during the third impact under the prestress of 25 MPa was 757.2 με, which is a 71.7% increase compared to the first impact. This is because the damage of the anchor solid under cyclic dynamic load under lower prestress (15 MPa) is in

a stable accumulation stage, whereas under higher prestress (25 MPa), the dynamic load induces accelerated damage to the anchor solid specimen, leading to a rapid increase in strain.

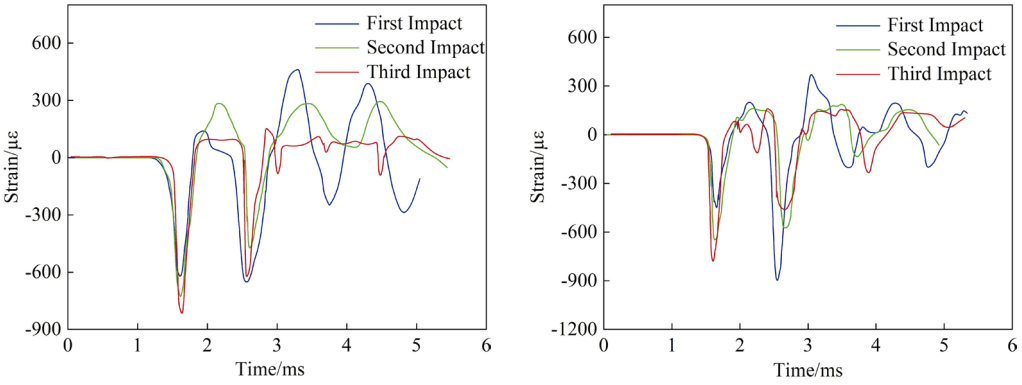

(a) Prestress 15 Mpa (b) Prestress 25 Mpa

Fig. 6. Strain time history curve of the free section under multiple impacts

A comparison of the time history curves of the strain distribution in the surrounding rock of the anchoring section, surrounding rock of the free section, and anchor bolt of the anchoring section in the anchoring solid is shown in Fig. 7. The peak value of the stress wave on the anchor bolt in the anchoring section appears on the third stress wave, with a peak value of 1471 με. The magnitude of the first, second, fourth, and fifth strain peaks is approximately 400 με; however, the peak strain in the surrounding rock at the anchorage section is only at the first and second strain peaks, which are approximately 500 με. At the first two peaks of the strain curve, the direction of the stress wave on the anchor bolt and the surrounding rock at the anchorage section is opposite, showing a strong "time difference effect", which is not related to the strength of the prestress, but is caused by the mismatch in the deformation of the anchor bolt and the surrounding rock. In the first two cycles, the size of the stress wave in the surrounding rock of the free

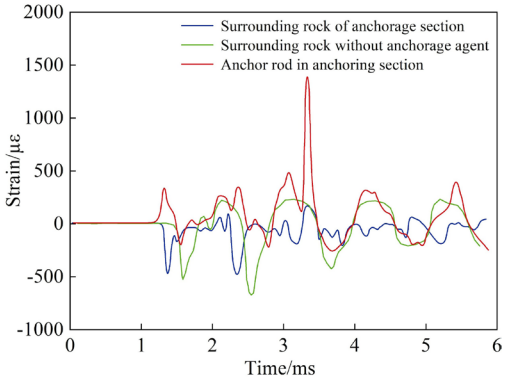

Fig. 7. Strain contrast curves of different positions in anchorage support

section is almost the same as that in the anchoring section. However, the stress wave in the free section lags behind that in the anchoring section because the anchoring section is far away from the impact end. The action time of the strain wave in the surrounding rock of the free section is significantly longer than that in the anchoring section, indicating that increasing the anchoring length can reduce the action time of the stress wave.

3.3. Laws of axial force loss of anchor rod under dynamic load

Under the action of dynamic loads, the anchor solid specimen cracks under the combined action of prestressing and dynamic load, especially at the anchorage interface, and the tension shear effect of the dynamic and static loads is more evident. In addition, the stress distribution of the surrounding rock at the contact interface between the anchor plate and the surrounding rock is uneven; this is prone to failure. However, the damage to the anchoring interface or looseness of the anchor plate causes loss of the anchor axial force. To quantitatively study the variation characteristics of the anchor strength under dynamic loads, a hydraulic dynamometer was used for monitoring during this test.

TABLE 2

Comparison table of axial force before and after a single impact

Initial axial force /MPa	15	17	25	30
Axle force after impact /MPa	11.57	12.38	15.22	12.36
Axial force loss rate %	23	26	40	60

Under various pre-stressed states, the axial force change of the anchor rod under a single impact is shown in TABLE 2; we can obtain the relationship between the prestress loss rate and the impact prestress on the anchor bolt. As shown in Fig. 8, when the anchor solid specimen experiences an impact, the axial force loss rates of the anchor corresponding to initial prestresses of 15, 17, 25, and 30 MPa are 23%, 26%, 40%, and 60%, respectively. The results show that the axial force loss rate increases with prestressing, and the loss value exhibits a secondary growth relationship.

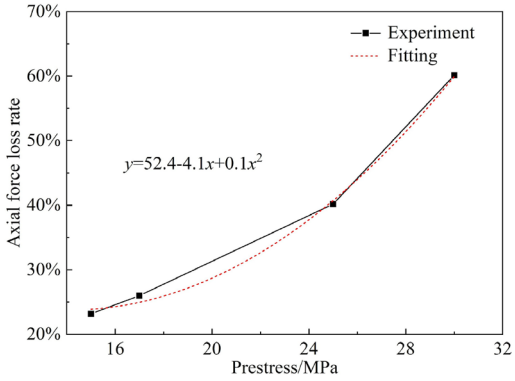

Fig. 8. Axial force loss curve of different prestressed anchors under impact

Axial force loss curve of anchor rod in anchor solid with prestress of 15, 17, 25, and 30 MPa under multiple impacts, as shown in Fig. 9. The axial force in the anchor rod decreases significantly after multiple impact loads. When the prestress values are 15 and 17 MPa, the axial force of the specimen decreases slowly, and when the prestress values are 25 and 30 MPa, the axial force of the specimen decreases rapidly. From the slope of the curve after impact, it can be seen that the greater the prestress in the anchor, faster the axial force reduction rate and fewer times the anchor failure needs. The above analysis shows that when the prestress is 17 MPa, the anchoring effect of the anchoring specimen is better, because the axial force loss of the anchor bolt is small under this prestress.

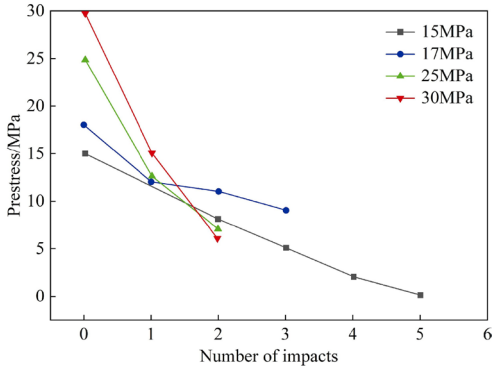

Fig. 9. Axial force loss curve of the bolt under multiple impacts

3.4. Damage characteristics of test piece under dynamic load

The failure characteristics of the impact end of the test piece are shown in Fig. 10. After the first and second impacts, there is no evident external damage at the impact end of the test piece. When the third impact occurs, a shear-peeling fracture occurs near the end of the impact end of the test piece. The impact causes damage to the end of the test piece. With an increase in the impact time, the damage increases and accumulates continuously, and when the damage reaches a certain threshold, macroscopic fracture occurs. The amount of damage at the end of the impact end caused by each impact is different, and the number of times the end is cracked depends entirely on the cumulative amount of damage. As shown in Fig. 9, as the number of impacts increases, the axial force gradually decreases and the damage gradually increases.

The spalling-failure characteristics of the surrounding rock at the free end are shown in Fig. 11. The surrounding rock at the free end is easily damaged because of the incident and reflected stresses at the contact surface. No binding forces are observed around the specimen. The failure form of the surrounding rock at the free end is from the outer to inner side. The free end of the specimen undergoes tensile failure under impact, as shown in Fig. 11(b). The primary reason for this failure is that the force on the end face is uneven owing to the flatness or material differences of the end face. The damage to the free-end face is related to the size of the impact dynamic load and to the number of impacts. With an increase in the number of impacts, the amount of surrounding rock peeled at the free end gradually increases, and the tension cracks continue to increase.

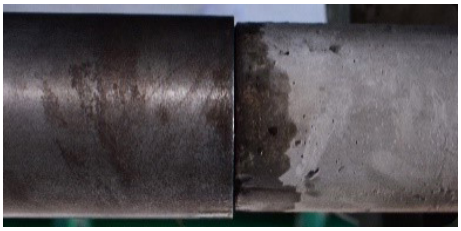

(a) First Impact

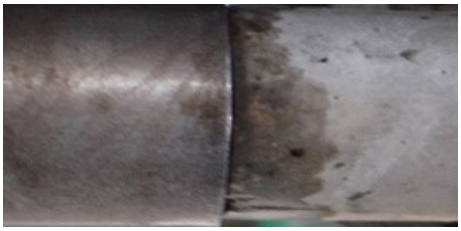

(b) Second Impact

(c) Third Impact

Fig. 10. Damage and failure characteristics of incident end

(a) Spalling failure

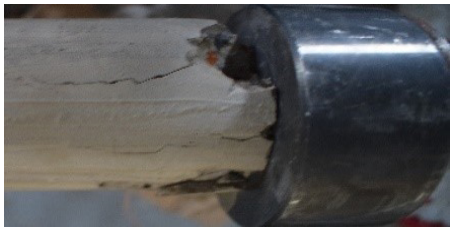

(b) Tensile failure

Fig. 11. Fracture characteristic of the transmissive end

Impact tests were performed on the anchoring test pieces under different prestresses and a digital camera was used to record the macro damage location and quantity in each test piece, as shown in Fig. 12, where I, II, and III represent the first, second, and third impacts, respectively. When the prestress is small, there are many cracks in the surrounding rock of the free section and damage at the impact end occurs after the third impact. When the prestress is large, there is only one fracture in the surrounding rock of the free section and the damage at the impact end occurs in the second impact. By comparing the fracture characteristics of the specimens under different prestresses, regardless of the prestress value, the surrounding rock of the anchorage section has no macroscopic fracture, indicating that increasing the anchorage length can effectively control the fracture of the surrounding rock. In addition, the length of the initial fracture is affected by the prestress value. When the prestress values are 15, 17, 25, and 30 MPa, the initial fracture lengths are 14.18, 14.48, 42.96, and 58.54 cm, respectively. With an increase in prestress, the initial fracture length of the anchor specimen increases gradually, which indicates that an increase in prestress in the side reaction can increase the strength of the surrounding rock in the anchorage zone.

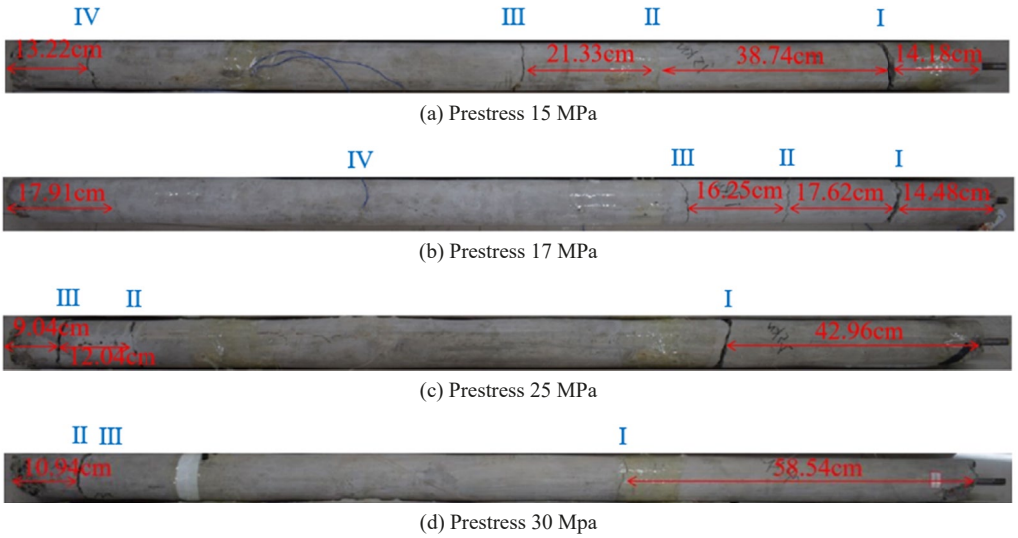

(a) Prestress 15 MPa

(b) Prestress 17 MPa

(c) Prestress 25 MPa

(d) Prestress 30 Mpa

Fig. 12. Failure characteristics of anchorage specimens

3.5. Effectiveness of roadway rock control

In order to avoid stress concentration and ensure the stability of the surrounding rock of the roadway, blasting pre splitting and roof cutting were adopted in the transportation roadway of the 11503w working face. However, blasting presents a typical dynamic load phenomenon on the roadway. Therefore, before the backfilling of the 11503w working face, pre drilling and energy gathering blasting should be carried out on the side of the coal wall along the groove to explore the support effect of prestressed anchor rods. The layout of top drilling along the groove is shown in Figs. 13(a) and 13(b). According to the lithology and thickness of the top rock layer of the working face, the average thickness of the two groups of rock layers is 6.85 m. To ensure the smooth collapse of the cut roof, the angle of the borehole is 70°. Therefore, the drilling depth is determined to be 6m, the borehole diameter is 36 mm, and the borehole spacing is 1 m. According to general considerations, the sealing length should be 0.25~0.3 of the total length of the borehole. The preliminary design sealing length is 1.5 m, the charging length is 4.5 m, and the charging structure is "2+2+1". The support method is anchor rod+anchor net+anchor cable support. The top plate and two sides both use anchor rods with a diameter of 22 mm and a length of 2000 mm. The top plate is reinforced with two anchor cables with a length of 6300 mm and a spacing of 1000 mm, Steel strips and anchor nets are arranged on the surface of the tunnel, and the support design cross-section is shown in Fig. 13(c).

The total length of the mining roadway in the 11503w working face is 650 m. Segmented blasting is used, and 17 MPa prestressed anchor rods are used to anchor the roadway. After each blasting, the displacement data of the two sides of the roadway is measured and recorded using a mining laser rangefinder. The displacement data on both sides of the roadway after three rounds of blasting is shown in Fig. 14. With the increase of blasting times, it was found that the displacement on both sides of the tunnel can be controlled within 0.3 m, and the average displacement on both sides of the tunnel is 206 mm, 240 mm, and 283 mm, respectively, increasing by 16.5%

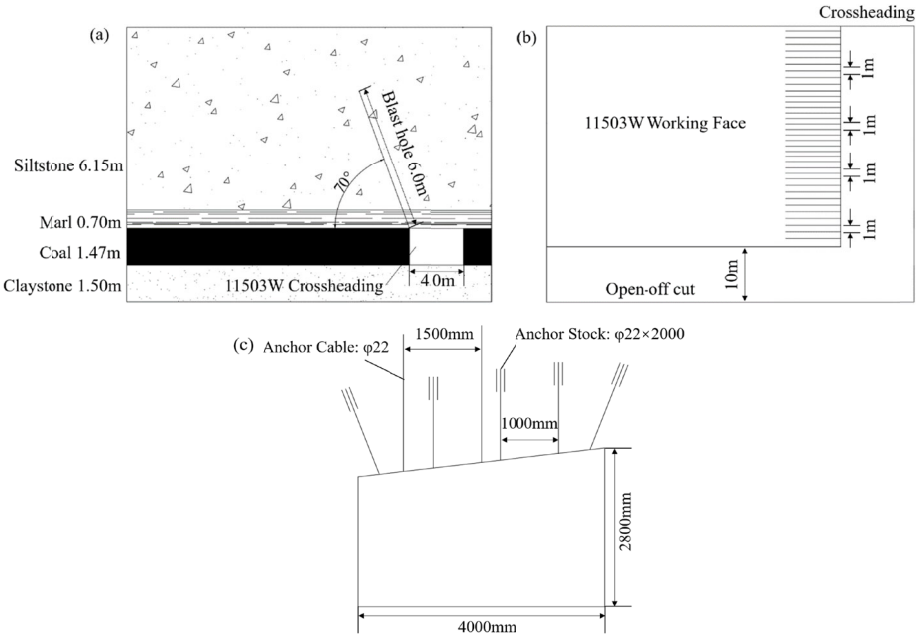

Fig. 13. Schematic diagram of roadway anchor support

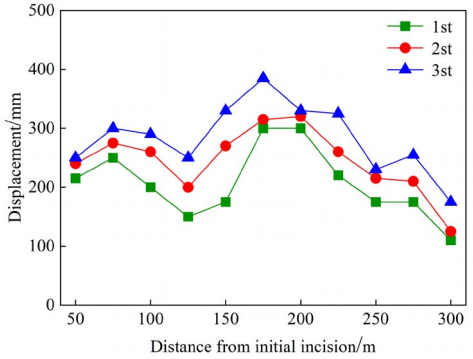

Fig. 14. Displacement of the two sides of the tunnel

and 17.9%, with a relatively low growth rate. Therefore, the practice of this project shows that the 17 MPa prestressed anchor rod support system can effectively control the deformation of both sides and maintain the stability of the surrounding rock of the tunnel.

4. Conclusion

In this study, the influence mechanism of anchorage prestress on stress wave transmission under dynamic loads was presented. The impact loading and static pull-out tests were carried

out on the specimens by making concrete anchorage specimens; the stress wave transmission law, axial force loss law, and failure characteristics of prestressed anchorage specimens were discussed and analyzed. The influence of the dynamic load on the pull-out strength of the anchor specimen was further determined through a pull-out test, and the following conclusions are drawn.

(1) In the prestress range of 15-30 MPa, with an increase in prestressing, the peak value of the stress wave in the surrounding rock of the anchor increases gradually, and the wave attenuation speed decreases. When the prestress values are 15 and 25 MPa, with an increase in the number of impacts, the damage to the surrounding rock of the anchor increases, prestress decreases, peak value of the stress wave increases, and attenuation speed of the stress wave accelerates.

(2) Under impact, the impact end of the prestressed anchorage specimen is sheared and the free end of the specimen is subjected to a combined tension and shear failure with a fracture in the middle. With an increase in the number of impacts, the degree of damage to the surrounding rock of the anchor increases. Increasing the prestress can reduce the number of fractures in the middle of the specimen.

(3) The strength of the prestressed anchor specimen after impact was lower than that of the anchor solid specimen without impact. Evaluation of the axial force loss in the test revealed that the residual axial force of the anchor was the largest at 17 MPa and the bolts exhibited the best dynamic adaptability.

(4) On site, a 17 MPa prestressed anchor rod was used to support the 11503w working face, and the displacement changes on the two sides of the tunnel were measured after three explosions. Under the 17 MPa prestressed force, the average displacements on both sides of the tunnel were 206, 240, and 283 mm, thus increasing by 16.5% and 17.9%.

This experiment primarily studied the damage to the anchors under different impact times and preloads. However, in actual coal mining, the surrounding rock is not in a uniform stress environment. There is huge scope for further research about stress wave propagation under gradient confining pressure.

Acknowledgments

This research was supported by the Outstanding Youth Research Program for Universities in Anhui Province (2023AH020025) and the National Natural Science Foundation of China (No. 522740070, 51874006).

References

[1] W. Korzeniowski, K. Skrzypkowski, L. Herezy, Laboratory method for ev aluating the characteristics of expansion rock bolts subjected to axial tension. Archives of Mining Sciences **60**, 1, 209-224 (2022). DOI: https://doi.org/10.1515/amsc-2015-0014

[2] K. Skrzypkowski, Laboratory testing of a long expansion rock bolt support for energy-absorbing applications. E3S Web of Conferences 9, 00004 (2018). DOI: https://doi.org/10.1051/e3sconf/20182900004

[3] M. Sharifzadeh, J.F. Luo, B. Crompton, Dynamic performance of energy-absorbing rockbolts based on laboratory test results. Part I: Evolution, deformation mechanisms, dynamic performance and classification. Tunnelling and Underground Space Technology **105**, 103510 (2020). DOI: https://doi.org/10.1016/j.tust.2020.103510

[4] Y. Yokota, Z.Y. Zhao, W. Nie, K. Date, K. Iwano, Y. Okada, Experimental and Numerical Study on the Interface Behaviour Between the Rock Bolt and Bond Material. Rock Mechanics and Rock Engineering **52**, 869-879 (2019). DOI: https://doi.org/10.1007/s00603-018-1629-4

[5] I. Coşkun, H. Engin, A. Özmutlu, Dynamic stress and displacement in an elastic half-space with a cylindrical cavity. Shock and Vibration **18**, 827-838 (2011). DOI: https://doi.org/10.3233/SAV-2010-0602

[6] H.E. Lawson., D. Tesarik, M.K. Larson, H. Abraham, Effects of overburden characteristics on dynamic failure in underground coal mining. International Journal of Mining Science and Technology **27**, 121-129(2017). DOI: http://dx.doi.org/10.1016/j.ijmst.2016.10.001

[7] N. Yugo, W. Shin, Analysis of blasting damage in adjacent mining excavations. Journal of Rock Mechanics and Geotechnical Engineering **7**, 282-290 (2015). DOI: http://dx.doi.org/10.1016/j.jrmge.2014.12.005

[8] X. Yi, P.K. Kaiser, Impact Testing for Rockbolt Design in Rockburst Conditions. Int. J. Rock Mech. Min. Sci. & Geomech. Abstr. **31**, 6, 671-685 (1994).

[9] A. Ansell, Laboratory testing of a new type of energy absorbing rock bolt. Tunnelling and Underground Space Technology **20**, 291-300 (2005). DOI: https://doi.org/10.1016/j.tust.2004.12.001

[10] A.H. Aliu, B. Abass, T. Fred, Impact load effects on screw anchors in concrete. Engineering Structures **251**, 113491 (2022). DOI: https://doi.org/10.1016/j.engstruct.2021.113491

[11] C.L.Charlie, D. Chantale, Performance of D-Bolts Under Dynamic Loading. Rock Mech. Rock Eng. **45**, 193-204 (2012). DOI: https://doi.org/10.1007/s00603-011-0202-1

[12] G. Solomos, M. Berra, Testing of anchorages in concrete under dynamic tensile loading. Materials and Structures **39**, 695-706 (2006). DOI: https://doi.org/10.1617/s11527-006-9112-1

[13] Y.H. Wu, X.S. Liu, Y.L. Tan, Q. Ma, D.Y. Fan, M.J. Yang, X. Wang, G.Q. Li, Mechanical Properties and Failure Mechanism of Anchored Bedding Rock Material under Impact Loading, Materials **15**, 6560 (2022). DOI: https://doi.org/10.3390/ma15196560

[14] F. Tahmasebinia, C.G. Zhang, I. Canbulat, O. Vardar, S. Saydam, Numerical and analytical simulation of the structural behaviour of fully grouted cable bolts under impulsive loading. International Journal of Mining Science and Technology **28**, 807-811 (2018). DOI: https://doi.org/10.1016/j.ijmst.2018.08.012

[15] N.I. Aleksandrova, M.V. Ayzenberg-Stepanenko, E. . Sher, Modeling the elastic wave propagation in a block medium under the impulse loading. Journal of Mining Science **45**, 2, 21-32(2009). DOI: https://doi.org/10.1007/s10913-009-0054-1

[16] J.A. Vallejos, E. Marambio, L. Burgos, C.V. Gonzalez, Numerical modelling of the dynamic response of threadbar under laboratory-scale conditions. Tunnelling and Underground Space Technology **100**, 103263 (2020). DOI: https://doi.org/10.1016/j.tust.2019.103263

[17] Y.J. Kim, R.G. Wight, M.F. Green, Flexural Strengthening of RC Beams with Prestressed CFRP Sheets: Development of Nonmetallic Anchor Systems. Journal of Composites for Construction **12**, 1, 35-43 (2008). DOI: https://doi.org/10.1061/(ASCE)1090-0268(2008)12:1(35)

[18] X. Gao, J.Q. Jia, G.X. Mei, X.H. Bao, L.H. Zhang, X.P. Liao, A New Prestress Loss Calculation Model of Anchor Cable in Pile-Anchor Structure. Mathematics **10**, 1260 (2022). DOI: https://doi.org/10.3390/math10081260

[19] L. Guo, X.A. Dong, Z. Wang, H. Li, Y.L. Sun, Analysis of Re-T ensioning Time of Anchor Cable Based on New Prestress Loss Model. Engineering Mathematics **9**, 1094 (2021). DOI: https://doi.org/10.3390/math9101094

[20] C. Burton, P. Visintin, M. Griffith, J. Vaculik, Stress wave foundation, Laboratory investigation of pull-out capacity of chemical anchors in individual new and vintage masonry units under quasi-static, cyclic and impact load. Structures **34**, 901-930 (2021). DOI: https://doi.org/10.1016/j.istruc.2021.08.016

[21] P.A. Persson, The relationship between strain energy, rock damage, fragmentation, and throw in rock blasting. Fragblast **1**, 99-110 (1997). DOI: https://doi.org/10.1080/13855149709408392